CMS Physics Analysis Summary

Contact: cms-pag-conveners-top@cern.ch 2016/05/07

Measurement of the differential cross section for t-channel single-top-quark production at $\sqrt{s} = 13$ TeV

The CMS Collaboration

Abstract

A measurement of differential cross sections for t-channel single-top-quark production in proton-proton collisions at a centre-of-mass energy of 13 TeV is presented. The cross sections are measured as functions of the transverse momentum and the absolute value of the rapidity of the top quark. The analyzed data were recorded in the year 2015 by the CMS experiment and correspond to an integrated luminosity of 2.3 fb^{-1}. A maximum-likelihood fit to a multivariate discriminator is used to infer the signal and background fractions from the data. Unfolding to parton level is performed. The measured cross sections are compared with theoretical predictions to next-to-leading order matched with parton showering as implemented in Monte Carlo generators. General agreement is found within uncertainties.

1 Introduction

The electroweak production of single top quarks has been discovered and established by measurements at the Fermilab Tevatron [1, 2] and the CERN LHC [3–7]. A variety of theory calculations and Monte Carlo (MC) generator programs exist that predict the cross section and properties of single-top quark production, within the standard model (SM) and beyond, using different approaches and approximations. Differential measurements of production cross sections are particularly well suited to assess the validity of the predictions.

The normalized differential cross sections of t-channel single-top-quark production, presented in this note, are measured as a function of the transverse momentum (p_{T}) and the absolute value of the rapidity ($y = \frac{1}{2}\ln\left[(E + p_z)/(E - p_z)\right]$) of the top quark. Figure 1 shows the corresponding Born-level Feynman diagrams of the production process in the 4 flavour (4FS) and 5 flavour schemes (5FS) which differ in the exclusion or inclusion of the b quark in the parton distribution function (PDF) [8]. This can contribute to differences in the predicted shapes of the top quark p_{T} and y as reported in Ref. [9] for LHC energies.

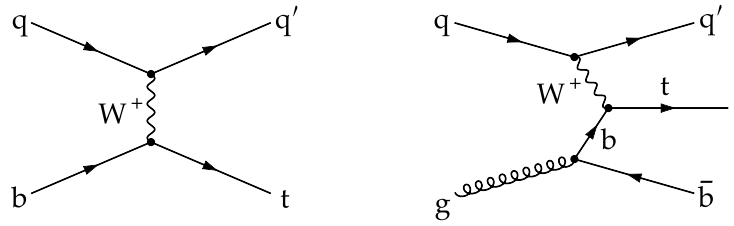

Figure 1: Born-level Feynman diagrams for single top quark production in the t channel: (left) (2)→(2) and (right) (2)→(3) processes. Corresponding diagrams exist for single-top-antiquark production.

Data corresponding to an integrated luminosity of 2.3 fb^{-1} recorded by the CMS experiment in proton-proton collisions at the LHC at a centre-of-mass energy of 13 TeV are analyzed. The measurement is restricted to events in which the top quark decays into a final state containing a b quark, a muon and a neutrino. Similar analyses have been reported by the ATLAS collaboration at a centre-of-mass energy of 7 TeV [5] and by the CMS collaboration at a centre-of-mass energy of 8 TeV [10].

This note is organized as follows: The dataset and simulated samples are described in Section 2; details on the event selection are given in Section 3; the reconstruction of a top-quark candidate and the fit procedure to estimate the signal and the background composition in data are discussed in Section 4; the methodology to infer the differential cross sections at parton level is presented in Section 5; the statistical procedure and the sources of systematic uncertainties affecting the measurement are detailed in Section 6; the results are given in Section 7; a summary is provided in Section 8.

2 Data and simulation

Proton-proton collision data delivered by the LHC with a bunch spacing of 25 ns at $\sqrt{s} =$ 13 TeV in the year 2015 are used for the measurement. The analyzed dataset, recorded when all CMS sub-detectors and the solenoid were fully operational, corresponds to an integrated luminosity of 2.3 fb^{-1} [11].

Samples containing simulated events of signal and background processes are used to compare

data with theoretical predictions. The signal process of t-channel single-top-quark production is simulated using the MC event generator MG5_aMC@NLO version 2.2.2 [12]. It is interfaced to PYTHIA version 8.205 [13, 14] for the simulation of hadronization and parton showering in the 4 flavour scheme (4FS) using the CUETP8M1 tune [15]. Alternative samples of the signal process are generated for comparisons using MG5_aMC@NLO interfaced with PYTHIA in the 5FS, POWHEG version 1 interfaced with PYTHIA in the 4FS [16], and MG5_aMC@NLO interfaced with HERWIG [17] in the 4FS where the latter uses the EE5C tune [18]. The background contribution from top-quark pair production ($\mathrm{t\bar{t}}$) is simulated using POWHEG version 2 [19, 20], interfaced to PYTHIA. The simulation of single-top-quark production in the tW channel uses POWHEG version 1 interfaced with PYTHIA. For all these samples a top-quark mass of 172.5 GeV is used. The MG5_aMC@NLO generator interfaced with PYTHIA is also used to generate background events from the production of W or Z bosons in association with jets (W+jets, Z/γ^*+jets).

The simulated events are overlaid with additional collision interactions ("pileup") according to the distribution inferred from the data. All generated events undergo a full GEANT4 [21] simulation of the detector response.

The single-top-quark production cross sections, calculated at next-to-leading order (NLO) using the HATHOR library version 2.1 [22], are $136.0^{+5.4}_{-4.6}$ pb for top quark and $81.0^{+4.1}_{-3.6}$ pb for top antiquark production via the t channel, and 71.7 ± 3.8 pb for inclusive production in the tW channel. The quoted uncertainties include scale and PDF variations. The predicted $\mathrm{t\bar{t}}$ production cross section is 832^{+20}_{-29} pb as calculated with the TOP++2.0 program to next-to-next-to-leading order in perturbative QCD, including soft-gluon resummation to next-to-next-to-leading-log (see Ref. [23] and references therein).

Differential $\mathrm{t\bar{t}}$ cross section measurements [24–26] have shown that the p_{T} spectrum of top quarks in $\mathrm{t\bar{t}}$ events is significantly softer than the one generated in simulation. To correct for this effect, simulated $\mathrm{t\bar{t}}$ events are reweighted according to scale factors derived from these measurements.

Although the cross section for production of multijet events is very large, the probability for a simulated event to mimic the final state of the signal process is very small. As a result it becomes impractical to simulate a sufficiently large number of events for this process. Therefore, multijet events are modelled using the shape of the data in a multijet-event-enriched sideband region. The method used to model the shape and estimate the yield of multijet events in data is detailed in Section 4.

3 Event selection

The signature of t-channel single-top-quark production where the top quark decays as $\mathrm{t} \to \mathrm{b}\mu\nu$ consists of one isolated muon, one b jet, one spectator jet (j') from a light-flavoured quark (u, d, or s), and missing transverse energy. The signature can feature a second b jet from initial state gluon splitting. In most events this second b jet is outside of the detector acceptance because its transverse momentum is small. Another characteristic of the signal process is that the light-flavoured quark recoils against the W boson. As a consequence, the spectator jet is often scattered into the forward detector region.

Data events are recorded by a trigger requiring the presence of an isolated muon with a transverse momentum of at least 20 GeV within a pseudorapidity range of $|\eta| < 2.4$. Events are reconstructed with the particle-flow (PF) algorithm [27, 28]. Single particles are reconstructed and identified by combining information from various detector components.

For the analysis the presence of exactly one isolated muon candidate with transverse momentum of $p_{\mathrm{T}} > 22$ GeV is required, detected within the trigger acceptance and fulfilling a set of additional muon identification criteria [29]. The relative muon isolation, $I^{\mu}_{\text{rel.}}$, is defined by

$$I^{\mu}_{\text{rel.}} = \frac{I_{\text{ch. had.}} + \max\left(I_{\gamma} + I_{\text{neut. had.}} - \frac{1}{2} \cdot I_{\text{PU}},\ 0\right)}{p^{\mu}_{\mathrm{T}}}, \tag{1}$$

where the charged hadron ($I_{\text{ch. had.}}$), photon (I_{γ}), and neutral hadron ($I_{\text{neut. had.}}$) transverse energy deposits are corrected by subtracting half of the scalar p_{T} sum from reconstructed tracks which are associated to pileup vertices, I_{PU}, within a cone of $\Delta R = \sqrt{\Delta\eta^2 + \Delta\phi^2} < 0.4$ around the muon.

Events with one well isolated muon that is required to have $I^{\mu}_{\text{rel.}} < 6\%$ are used in the measurement. Muons with $I^{\mu}_{\text{rel.}} > 20\%$ will be referred to as anti-isolated. The latter usually originate from multijet production.

Events with one or more additional muons or electrons are rejected. The criteria used to identify additional leptons are loosened and in addition the following requirements are applied: $p_{\mathrm{T}} > 10(20)$ GeV and $|\eta| < 2.5(2.5)$ for muons (electrons). Loose muons are furthermore required to have $I^{\mu}_{\text{rel.}} < 20\%$. Loose electrons are additionally required to fulfil dedicated quality criteria that are specifically designed for vetoing electrons.

Jets are clustered from PF candidates using the anti-k_t algorithm [30] with a distance parameter of $R = 0.4$. The influence of pileup is mitigated using the charged hadron subtraction (CHS) technique [31]. Jets are rejected if $\Delta R(\text{jet}, \mu) < 0.3$ in order to avoid overlap of the jets with the selected muon candidate. The jet energy and resolution is corrected to account for the non-flat detector response in η and p_{T} of the jet. Corrected jets with transverse momenta of $p_{\mathrm{T}} > 40$ GeV and within $|\eta| < 4.7$ are selected. Forward jets ($|\eta| > 3$) are required to have an electromagnetic energy fraction smaller than 90% and to be constructed from more than ten PF candidates. For central jets ($|\eta| < 3$) the following criteria are imposed: The neutral electromagnetic and hadronic energy fractions are both required to be $< 99\%$ and the jet is required to consist of more than one PF candidate. Furthermore, if the jet falls into the tracker acceptance ($|\eta| < 2.4$), the charged hadron energy fraction and multiplicity should both be > 0 and the charged electromagnetic energy fraction should be $< 99\%$.

The multivariate b-tagging discriminator "Combined Secondary Vertex Tagger" [32] is used to identify jets that originate from the hadronization of b quarks. A threshold is chosen that corresponds to a mistag rate of about 0.1% and a tagging efficiency of about 50% depending on the jet transverse momentum and pseudorapidity [33].

The missing transverse momentum is defined as the negative vectorial sum of all reconstructed PF candidates, $\vec{\not{p}}_{\mathrm{T}} = -\sum_i \vec{p}_i^{\,\text{PF}}$. Its magnitude, $\not{E}_{\mathrm{T}} = |\vec{\not{p}}_{\mathrm{T}}|$, is referred to as missing transverse energy. The energy scale and resolution corrections applied to the jets described above are propagated via the clustered PF candidates to the $\not{E}_{\mathrm{T}}$. This rebalances the transverse net momentum of the event and improves also the $\not{E}_{\mathrm{T}}$ resolution itself.

Although $\not{E}_{\mathrm{T}}$ is not directly used in the event selection, a threshold is applied on a closely related variable, i.e. the transverse W boson mass, defined as

$$m_{\mathrm{T}}(\mathrm{W}) = \sqrt{\left(p^{\mu}_{\mathrm{T}} + \not{E}_{\mathrm{T}}\right)^2 - \left(p^{\mu}_{x} + \not{p}_{\mathrm{T},x}\right)^2 - \left(p^{\mu}_{y} + \not{p}_{\mathrm{T},y}\right)^2} \tag{2}$$

where p_{T}^{μ} denotes the muon momentum. To reject events from multijet production, $m_{\mathrm{T}}(\mathrm{W}) > 50$ GeV must be fulfilled.

The number of selected jets and b-tags per event is used to define signal and control regions. The signal region is characterized by two jets and one b-tag (2j1t). Events from this region are used for the differential cross section measurement. A W+jets control region is defined by events with two non-tagged jets (2j0t) and a $\mathrm{t\bar{t}}$ control region is defined containing events with three jets and one or two b-tags (3j1t, 3j2t).

4 Background estimation and signal extraction

4.1 Top-quark reconstruction

The reconstruction of events assuming t-channel single-top-quark production starts with the reconstruction of the W boson from the selected muon and the missing transverse momentum. The p_z component of a neutrino candidate is found by imposing a W boson mass constraint on the sum of the muon and missing transverse energy 4-momenta as in Ref. [3]. In about two thirds of all signal events this approach results in two real solutions for the missing p_z component and the solution with the smallest absolute value of $|p_z|$ is chosen. For the remaining events, the reconstructed transverse W boson mass exceeds the mass constraint which leads to complex solutions. The imaginary part of the solution is eliminated by modifying the transverse components of the missing transverse momentum independently, yielding $m_{\mathrm{T}}(\mathrm{W}) = m_{\mathrm{W}}$. These choices are justified based on studies of simulated signal events.

A top-quark candidate can be unambiguously defined in the 2j1t signal region using the selected muon, the neutrino candidate and the b-tagged jet. The 4-momentum of the top-quark candidate (from which its mass, transverse momentum and rapidity are derived) is defined as the sum of 4-momenta of these reconstructed objects. The other, non-tagged jet is then interpreted as the light jet (j') originating from the spectator quark (q') which recoils against the W boson. In the control regions, the following scheme is used. First, b-tagged jets are sorted by p_{T} and non-tagged jets are sorted by $|\eta|$. Then, the most forward, non-tagged jet is taken as the light jet and the hardest b-tagged jet is associated to the top-quark decay. This is motivated by the fact that the spectator quark, in signal events, is often scattered into the forward detector region whereas additional b-tagged jets likely stem from initial state gluon splitting for which a much softer transverse momentum is expected compared to the b jet from the top-quark decay.

4.2 Background discrimination with a multivariate analysis

After the event selection, the amount of remaining background is still very high. To discriminate between signal and background events further, a Boosted Decision Tree (BDT) [34, 35] is trained to separate the dominant $\mathrm{t\bar{t}}$ and W+jets background from the signal process using as input various kinematic observables.

The BDT is trained using simulated events from the 2j1t region without imposing a selection on the transverse W boson mass. To prevent remaining multijet events that pass the $m_{\mathrm{T}}(\mathrm{W}) > 50$ GeV requirement to be classified as signal-like, simulated multijet events from the anti-isolated region are added to the training as background as well. The signal and background contributions are adjusted to the expectations from the maximum-likelihood fit as described in the next subsection.

Only discriminating observables that are well modelled in control and signal regions by the simulation are considered for the training. The five observables used as input to the BDT train-

ing are briefly described in the following. These have been carefully selected to have little correlation with the top quark p_T and rapidity such that data is not biased towards the signal SM prediction as a simulated SM signal sample is used for the training. The two most discriminating observables which are also well modelled by the simulation are the pseudorapidity of the non-tagged jet, $|\eta(j')|$, and the invariant mass of the reconstructed top-quark candidate, $m_{\mu\nu b}$, as shown in Fig. 2, top row. Further input observables are the ΔR distance between the two selected jets, the absolute difference in pseudorapidity between the b-tagged jet and the selected muon (Fig. 2, bottom row), and $m_T(W)$ (Fig. 3, left).

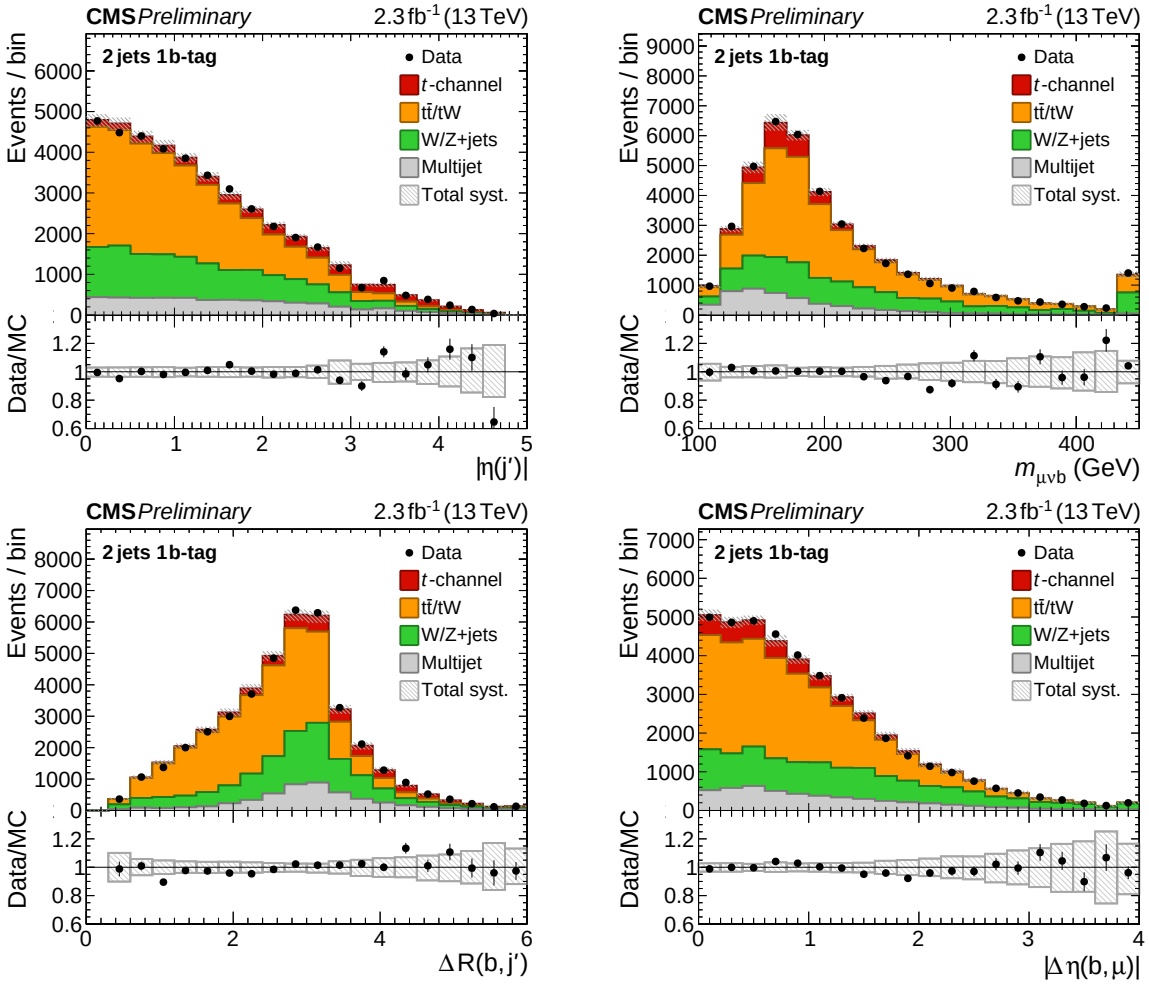

Figure 2: Distributions of discriminating observables used in the BDT training: (top left) the absolute value of the pseudorapidity of the non-tagged jet; (top right) the mass of the reconstructed top quark candidate; (bottom left) the ΔR distance between the two selected jets; (bottom right) the absolute difference in pseudorapidity between the b-tagged jet and the selected muon. The simulations of the different processes are normalized to the inclusive ML fit result. The ratio of yields in data and simulation is displayed under the histograms. The hatched band denotes the total systematic uncertainty scaled to the fit results. The first and last bin includes the under- and overflow of events, respectively.

The resulting BDT discriminant is shown in Fig. 3 for events with $m_T(W) > 50$ GeV. A good agreement between data and simulation is observed. The same discriminator obtained from training on events in the 2j1t region is evaluated also in control regions.

4.3 Maximum-likelihood fit

Binned maximum-likelihood fits are performed, separately in each bin of the measurement, using a combined likelihood by taking the $m_{\mathrm{T}}(\mathrm{W})$ distribution for events with $m_{\mathrm{T}}(\mathrm{W}) < 50\,\mathrm{GeV}$, and the BDT discriminant otherwise. The fits yield the fractions of signal and background contributions in data inclusively and differentially in intervals of the reconstructed top quark p_{T} and rapidity. The $m_{\mathrm{T}}(\mathrm{W})$ shape is a powerful handle to estimate the multijet event yield whereas the BDT discriminant provides sensitivity to the other backgrounds and to the signal yields.

In order to reduce the overall amount of parameters in the fits, similar processes are grouped together: tW and $\mathrm{t\bar{t}}$ are lumped into the $\mathrm{t\bar{t}}$/tW background, and W+jets and Z/γ^*+jets into the W/Z+jets background. The shape of multijet events is modelled using a template from anti-isolated muons in data. Log-normal priors with a conservative width of 30% (100%) are used to constrain the W/Z+jets (multijet) yields, respectively. A tighter constraint of 10% is used for the top-quark background yield as $\mathrm{t\bar{t}}$ production is much better understood in this particular analysis phase space. The signal yield is kept unconstrained.

The two $\mathrm{t\bar{t}}$-dominated control regions (3j1t, 3j2t) are included in the fits as well. In addition to providing better control of the $\mathrm{t\bar{t}}$ event yield, their inclusion is found to reduce the correlations between the estimated background yields. A good agreement with data is observed after scaling the simulated samples to the inclusive fit result. Figure 3 shows the corresponding distributions of the fit variables in the signal region.

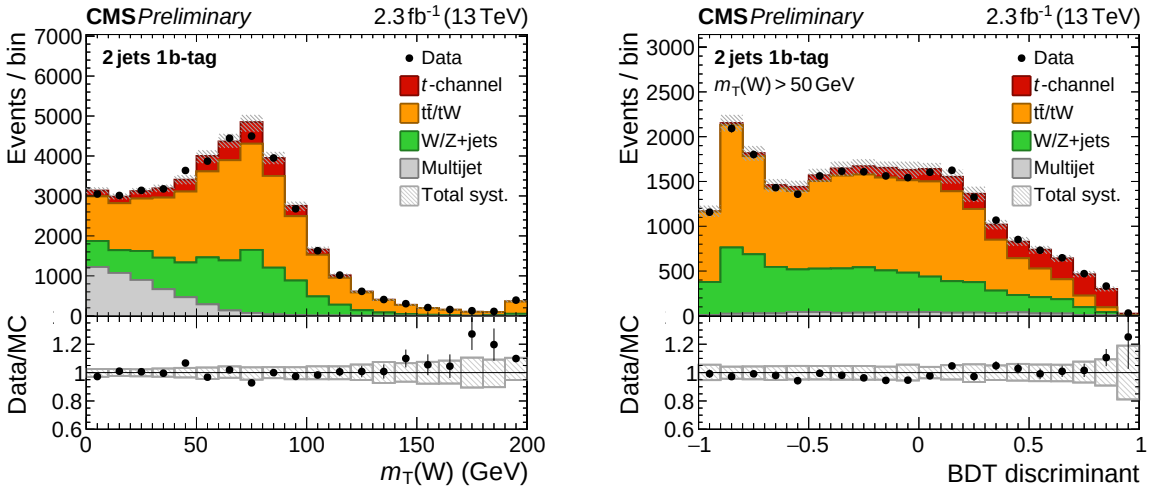

Figure 3: Distributions of the fit variables: (left) the transverse W boson mass distribution and (right) the BDT discriminant after selecting only events with $m_{\mathrm{T}}(\mathrm{W}) > 50\,\mathrm{GeV}$. The simulations of the different processes are normalized to the inclusive ML fit result. The ratio of yields in data and simulation is displayed under the histograms. The hatched band denotes the total systematic uncertainty scaled to the fit results. The first and last bin includes the under- and overflow of events, respectively.

5 Unfolding

The aim of this analysis is to measure the differential cross section of single-top-quark production as a function of the parton-level single top quark transverse momentum and rapidity. The reconstructed distributions are affected by detector resolution, selection efficiencies and kine-

matic reconstruction which lead to distortions with respect to the original event distributions. The size of these effects vary with the event kinematics. In order to infer the parton-level distributions, an unfolding method is applied to the reconstructed distributions, correcting for the mentioned distortion effects. In this analysis the TUNFOLD algorithm [36] is chosen which treats unfolding as a minimization problem. A penalty term, based on the resulting curvature of the unfolded spectrum [37, 38], is added in the minimization to reject oscillating solutions from amplified statistical fluctuations. This procedure is called "regularization" and its strength is chosen such as to minimize the global correlation between the unfolded bins.

The reconstructed distributions in a signal-depleted (signal-enhanced) phase space defined by $m_{\mathrm{T}}(\mathrm{W}) > 50$ GeV and BDT < 0 (BDT > 0.6) are shown in Fig. 4, respectively.

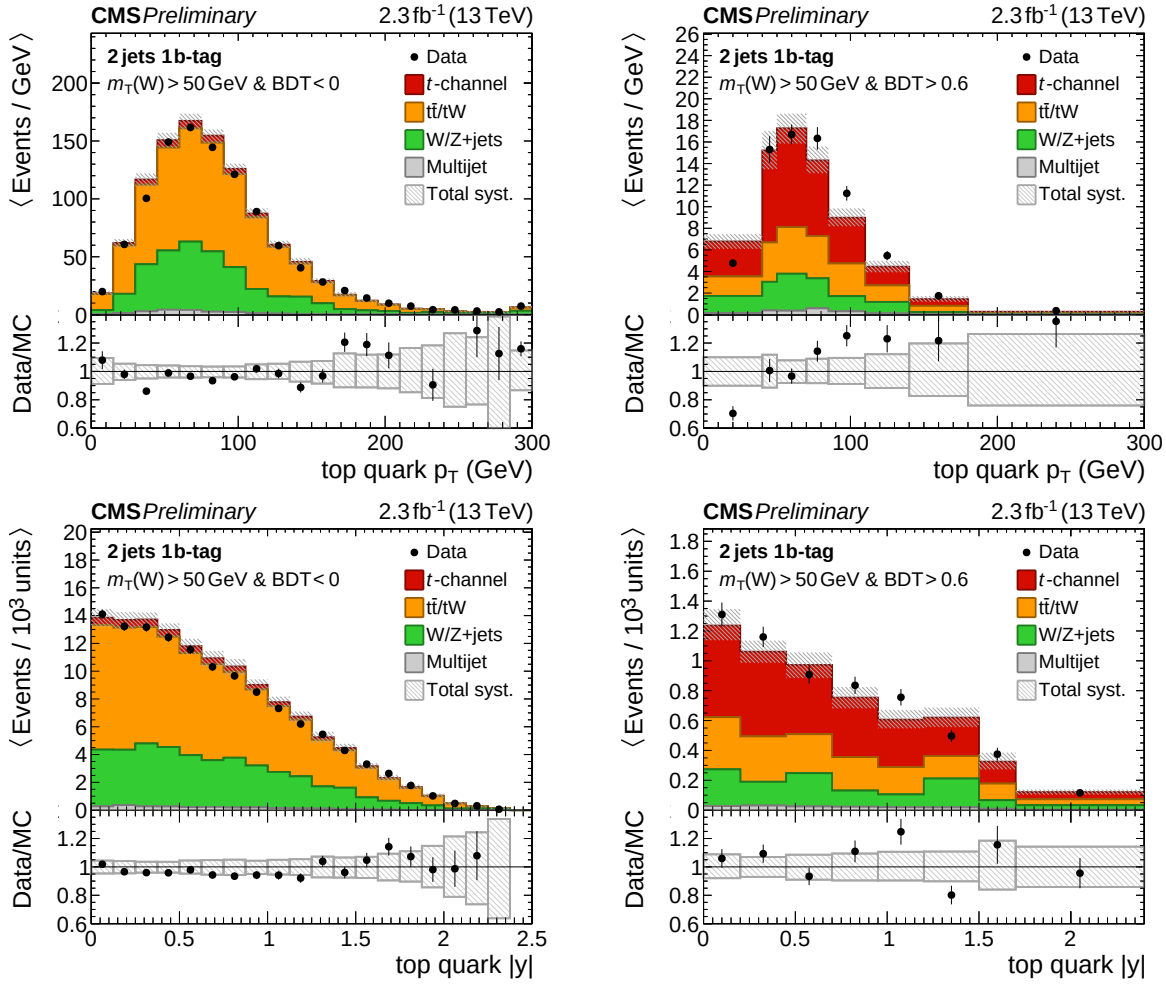

Figure 4: Distributions of (top row) the transverse momentum and (bottom row) the rapidity of the reconstructed top quark in 2j1t for events with $m_{\mathrm{T}}(\mathrm{W}) > 50$ GeV: (left column) signal-depleted region (BDT < 0), (right column) signal-enhanced region (BDT > 0.6). The simulations of the different processes are normalized to the inclusive ML fit result. The ratio of yields in data and simulation is displayed under the histograms. The hatched band denotes the total systematic uncertainty scaled to the fit results. The average number of events per bin is normalized to the bin width. The first and last bin includes the under- and overflow of events, respectively.

In the signal-depleted phase space, a good agreement between data and simulation for the

reconstructed top quark p_{T} and rapidity is observed which validates the background simulations. A good agreement is also observed for the rapidity in the signal-enhanced phase space. However, for the p_{T} distribution the data display a somewhat harder spectrum than the expectation.

For the unfolding, the signal yields are estimated from ML fits to the combined $m_{\mathrm{T}}(\mathrm{W})$ and BDT discriminant distributions, separately in exclusive top quark p_{T} and $|y|$ bins of the measurement. No selection on the BDT discriminant is applied.

The parton-level top quark is defined as the generated on-shell top quark after QED and QCD radiation, taking into account the intrinsic k_T of initial-state partons.

The binning is chosen such as to minimize the migrations between the reconstructed bins while retaining sensitivity to the shapes of the distributions. The stability (purity) are defined as the probabilities that the parton-level (reconstructed) values of an observable within a certain range also have their reconstructed (parton-level) counterparts in the same range. The size of the bins is chosen such that both quantities are larger than $\sim 50\%$.

The overall acceptance of signal events per unfolding bin after the 2j1t event selection ranges from 1.5% to 2.5% with the exception of the first top quark p_{T} (1.1%) and the last $|y|$ (0.7%) bins. Pseudo-experiments using simulated data are performed to verify that the unfolding method estimates the uncertainties correctly while keeping the bias at a minimum.

6 Systematic uncertainties

The measurement is affected by various sources of systematic uncertainty. For each systematic variation the whole analysis is repeated with replaced fit templates and response matrices.

The central value and total uncertainty of the cross section measurement are calculated from the combination of all variations. For this purpose, multiple Gaussian distributions, one per uncertainty source, are diced around the unfolded nominal template with a width corresponding to the difference between the unfolded systematic variation and the unfolded nominal result. The distribution of the sum of the diced yields is used to extract the final result. The central value is taken as the median and the total uncertainty as one standard deviation quantile.

In the following, the considered sources of systematic uncertainty and their impact on the measurement are described.

Background composition As described in Section 4.3, the Z/γ^*+jets, W+jets processes and $\mathrm{t\bar{t}}$, tW processes are grouped together in the ML fit. An additional uncertainty accounts for their assumed ratios. Each ratio is varied corresponding to a conservative $\pm 20\%$ variation of the Z/γ^*+jets or tW cross section.

Multijet shape estimation The shape of multijet events is estimated from data by inversion of the muon isolation criterion. An uncertainty on the shape is taken into account by changing the isolation range.

b tagging efficiency The scale factors used to reweight the b-tagging efficiency in simulation to the one estimated from data are varied within their uncertainties [39]. Twice the variation is applied to true charm jets taken to be 100% correlated to the true b jet scale factor. The scale factors for mistagged jets are varied independently.

Jet energy scale and resolution The jet energy scale and resolution corrections are varied within

their uncertainties. The shifts induced in the jet momenta are propagated to the missing transverse energy as well.

Pileup The distribution of pileup interactions is rederived by shifting the inelastic pp cross section by $\pm 5\%$.

Muon trigger, identification, and isolation efficiencies The scale factors accounting for the muon trigger, identification, and isolation efficiencies are varied within their uncertainties, including an additional systematic component that covers their dependence on the jet multiplicity.

Generator model The modelling of the signal process and the response matrix used for unfolding is taken as an additional uncertainty. A template is derived by changing the default generator from MG5_aMC@NLO to POWHEG.

Hadronization model The modelling of the hadronization simulation for the signal processes is taken as an additional uncertainty. A template is derived by changing the default hadronization simulation from PYTHIA to HERWIG.

Top quark mass An uncertainty on the top quark mass of $m = 172.5 \pm 1$ GeV is propagated to the unfolding by using dedicated $\mathrm{t\bar{t}}$, tW and t-channel samples with varied top-quark masses.

Parton distribution function The uncertainty on the PDF is estimated by reweighting simulated events according to all variations of the NNPDF3.0 set [40].

Renormalization and factorization scale A reweighting procedure of the simulated samples is applied using information stored in the event during the simulation of the hard scattering by the matrix element generator. These correspond to a coherent variation of a factor 2 (0.5) in renormalization and factorization scales with respect to the nominal values. Dedicated samples are produced to evaluate the effect of varying these scales, by the same factors, at parton shower level. We quote as an uncertainty the envelope of all possible combinations of up-varied / nominal / down-varied scales at matrix element and parton shower levels, with the exception of the extreme combinations up-varied matrix element scales / down-varied parton shower scales, and vice versa.

$\mathrm{t\bar{t}}$ p_{T} reweighting The measurement is performed without applying the $\mathrm{t\bar{t}}$ p_{T} reweighting as an estimate of the resulting uncertainty.

The sources of uncertainties which have the largest impact on the differential cross section measurements are the data statistics (10%-25%), the choice of the renormalization and factorization scale of the signal process (10%-15%), the top-quark mass (10%-20%) and the jet energy corrections (10%-15%).

7 Results

The unfolded distributions of the transverse momentum and the absolute value of the rapidity of the top quark are shown in Fig. 5, normalized to the in-situ measured inclusive cross section of t-channel single top-quark production. The data are compared to the SM expectations generated with MG5_aMC@NLO in the 4FS interfaced with PYTHIA 8, POWHEG in the 4FS interfaced with PYTHIA 8, MG5_aMC@NLO in the 5FS interfaced with PYTHIA 8, and MG5_aMC@NLO in the 4FS interfaced with HERWIG. The unfolded data distributions are, within the estimated

uncertainties, described by theoretical predictions. In the first top-quark p_T bin, the low acceptance to select signal events and the large sensitivity to the systematic uncertainties leads to a particularly large relative uncertainty. Within the current uncertainties, the data are described by the theoretical predictions.

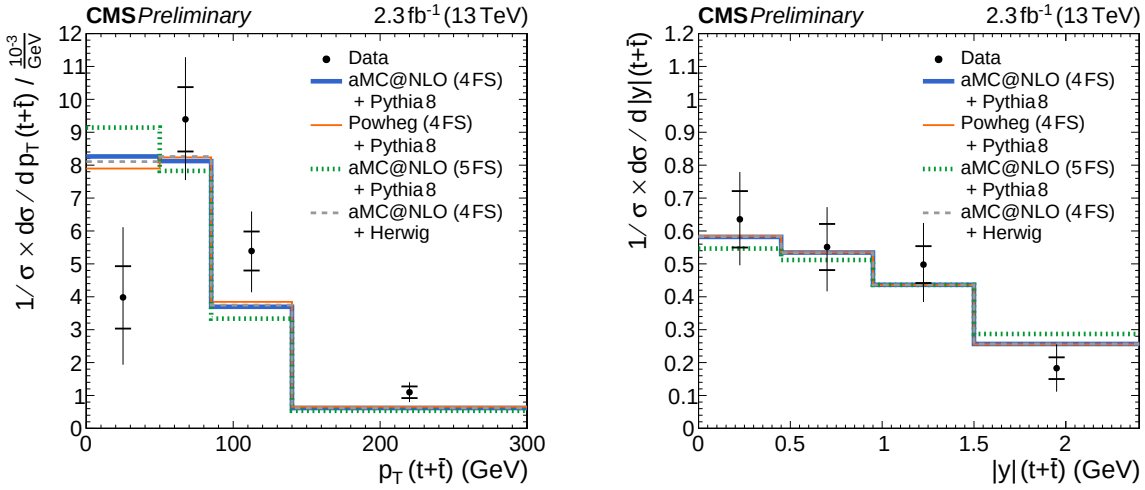

Figure 5: Measured differential cross section of t-channel single top quark production as a function of the top quark (left) transverse momentum and (right) rapidity. Horizontal ticks on the error bars indicate the statistical uncertainty and vertical bars indicate the total uncertainty per bin.

8 Summary

The differential cross section of t-channel production of single top quarks has been measured as a function of the transverse momentum and rapidity of the top quark using a dataset corresponding to a total integrated luminosity of 2.3 fb^{-1} at $\sqrt{s} = 13$ TeV, collected with the CMS detector. Within the experimental uncertainties, no significant deviation is observed with respect to the theoretical predictions based on NLO+PS generators in the 4FS or 5FS.

References

[1] CDF Collaboration, "First Observation of Electroweak Single Top Quark Production", *Phys.Rev.Lett.* **103** (2009) 092002, doi:10.1103/PhysRevLett.103.092002, arXiv:0903.0885.

[2] D0 Collaboration, "Observation of Single Top Quark Production", *Phys.Rev.Lett.* **103** (2009) 092001, doi:10.1103/PhysRevLett.103.092001, arXiv:0903.0850.

[3] CMS Collaboration, "Measurement of the t-channel single top quark production cross section in pp collisions at $\sqrt{s} = 7$ TeV", *Phys.Rev.Lett.* **107** (2011) 091802, doi:10.1103/PhysRevLett.107.091802, arXiv:1106.3052.

[4] ATLAS Collaboration, "Measurement of the t-channel single top-quark production cross section in pp collisions at $\sqrt{s} = 7$ TeV with the ATLAS detector", *Phys. Lett.* **B717** (2012) 330–350, doi:10.1016/j.physletb.2012.09.031, arXiv:1205.3130.

[5] ATLAS Collaboration, "Comprehensive measurements of t-channel single top-quark production cross sections at $\sqrt{s} = 7$ TeV with the ATLAS detector", *Phys. Rev.* **D90** (2014), no. 11, 112006, doi:10.1103/PhysRevD.90.112006, arXiv:1406.7844.

[6] CMS Collaboration, "Measurement of the single-top-quark t-channel cross section in pp collisions at $\sqrt{s} = 7$ TeV", *JHEP* **1212** (2012) 035, doi:10.1007/JHEP12(2012)035, arXiv:1209.4533.

[7] CMS Collaboration, "Measurement of the t-channel single-top-quark production cross section and of the V_{tb} CKM matrix element in pp collisions at $\sqrt{s}$= 8 TeV", *JHEP* **1406** (2014) 090, doi:10.1007/JHEP06(2014)090, arXiv:1403.7366.

[8] F. Maltoni, G. Ridolfi, and M. Ubiali, "b-initiated processes at the LHC: a reappraisal", *JHEP* **07** (2012) 022, doi:10.1007/JHEP04(2013)095, 10.1007/JHEP07(2012)022, arXiv:1203.6393. [Erratum: JHEP04,095(2013)].

[9] J. M. Campbell, R. Frederix, F. Maltoni, and F. Tramontano, "Next-to-Leading-Order Predictions for t-Channel Single-Top Production at Hadron Colliders", *Phys. Rev. Lett.* **102** (2009) 182003, doi:10.1103/PhysRevLett.102.182003, arXiv:0903.0005.

[10] CMS Collaboration, "Single top t-channel differential cross section at 8 TeV", CMS Physics Analysis Summary CMS-PAS-TOP-14-004, 2014.

[11] CMS Collaboration, "CMS Luminosity Measurement for the 2015 Data Taking Period", CMS Physics Analysis Summary CMS-PAS-LUM-15-001, 2016.

[12] J. Alwall et al., "The automated computation of tree-level and next-to-leading order differential cross sections, and their matching to parton shower simulations", *JHEP* **07** (2014) 079, doi:10.1007/JHEP07(2014)079, arXiv:1405.0301.

[13] T. Sjöstrand, S. Mrenna, and P. Z. Skands, "PYTHIA 6.4 Physics and Manual", *JHEP* **0605** (2006) 026, doi:10.1088/1126-6708/2006/05/026, arXiv:hep-ph/0603175.

[14] T. Sjöstrand, S. Mrenna, and P. Z. Skands, "A Brief Introduction to PYTHIA 8.1", *Comput. Phys. Commun.* **178** (2008) 852–867, doi:10.1016/j.cpc.2008.01.036, arXiv:0710.3820.

[15] CMS Collaboration, "Event generator tunes obtained from underlying event and multiparton scattering measurements", *Eur. Phys. J.* **C76** (2016), no. 3, 155, doi:10.1140/epjc/s10052-016-3988-x, arXiv:1512.00815.

[16] S. Alioli, P. Nason, C. Oleari, and E. Re, "NLO single-top production matched with shower in POWHEG: s- and t-channel contributions", *JHEP* **09** (2009) 111, doi:10.1007/JHEP02(2010)011, 10.1088/1126-6708/2009/09/111, arXiv:0907.4076. [Erratum: JHEP02,011(2010)].

[17] J. Bellm et al., "Herwig 7.0 / Herwig++ 3.0 Release Note", arXiv:1512.01178.

[18] M. H. Seymour and A. Siodmok, "Constraining MPI models using σ_{eff} and recent Tevatron and LHC Underlying Event data", *JHEP* **10** (2013) 113, doi:10.1007/JHEP10(2013)113, arXiv:1307.5015.

[19] S. Frixione, P. Nason, and C. Oleari, "Matching NLO QCD computations with Parton Shower simulations: the POWHEG method", *JHEP* **11** (2007) 070, doi:10.1088/1126-6708/2007/11/070, arXiv:0709.2092.

[20] S. Alioli, P. Nason, C. Oleari, and E. Re, "A general framework for implementing NLO calculations in shower Monte Carlo programs: the POWHEG BOX", *JHEP* **1006** (2010) 043, doi:10.1007/JHEP06(2010)043, arXiv:1002.2581.

[21] GEANT4 Collaboration, "GEANT4 - a simulation toolkit", *Nucl. Instrum. Meth. A* **506** (2003) 250, doi:10.1016/S0168-9002(03)01368-8.

[22] M. Aliev et al., "HATHOR: HAdronic Top and Heavy quarks crOss section calculatoR", *Comput. Phys. Commun.* **182** (2011) 1034–1046, doi:10.1016/j.cpc.2010.12.040, arXiv:1007.1327.

[23] M. Czakon and A. Mitov, "Top++: A Program for the Calculation of the Top-Pair Cross-Section at Hadron Colliders", *Comput.Phys.Commun.* **185** (2014) 2930, doi:10.1016/j.cpc.2014.06.021, arXiv:1112.5675.

[24] CMS Collaboration, "Measurement of the differential cross section for top quark pair production in pp collisions at $\sqrt{s} = 8$ TeV", *Eur. Phys. J.* **C75** (2015), no. 11, 542, doi:10.1140/epjc/s10052-015-3709-x, arXiv:1505.04480.

[25] CMS Collaboration, "Measurement of the inclusive and differential $\mathrm{t\bar{t}}$ production cross sections in lepton + jets final states at 13 TeV", CMS Physics Analysis Summary CMS-PAS-TOP-16-008, 2016.

[26] CMS Collaboration, "Measurement of the differential cross section for $\mathrm{t\bar{t}}$ production in the dilepton final state at $\sqrt{s} = 13$ TeV", CMS Physics Analysis Summary CMS-PAS-TOP-16-011, 2016.

[27] CMS Collaboration, "Particle-Flow Event Reconstruction in CMS and Performance for Jets, Taus, and $\not\!\!E_{\mathrm{T}}$", CMS Physics Analysis Summary PFT-09-001, 2009.

[28] CMS Collaboration, "Commissioning of the particle flow event reconstruction with the first LHC collisions recorded in the CMS detector", CMS Physics Analysis Summary PFT-10-001, 2010.

[29] CMS Collaboration, "Performance of CMS muon reconstruction in pp collision events at $\sqrt{s} = 7$ TeV", *JINST* **7** (2012) P10002, doi:10.1088/1748-0221/7/10/P10002, arXiv:1206.4071.

[30] M. Cacciari, G. P. Salam, and G. Soyez, "The anti-$\mathrm{k_t}$ jet clustering algorithm", *JHEP* **04** (2008) 063, doi:10.1088/1126-6708/2008/04/063, arXiv:0802.1189.

[31] CMS Collaboration, "Pileup Removal Algorithms", CMS Physics Analysis Summary CMS-PAS-JME-14-001, 2014.

[32] CMS Collaboration, "Identification of b-quark jets with the CMS experiment", *JINST* **8** (2013) 04013, doi:10.1088/1748-0221/8/04/P04013, arXiv:1211.4462.

[33] CMS Collaboration, "Identification of b quark jets at the CMS Experiment in the LHC Run 2", CMS Physics Analysis Summary CMS-PAS-BTV-15-001, 2016.

[34] L. Breiman, J. Friedman, R. A. Olshen, and C. J. Stone, "Classification and regression trees". Chapman and Hall/CRC, 1984.

[35] J. H. Friedman, "Recent advances in predictive (machine) learning", *J. Classif.* **23** (2006) 175–197, doi:10.1007/s00357-006-0012-4.

[36] S. Schmitt, "TUnfold: an algorithm for correcting migration effects in high energy physics", *JINST* **7** (2012) T10003, doi:10.1088/1748-0221/7/10/T10003, arXiv:1205.6201.

[37] A. Tikhonov, "Solution of Incorrectly Formulated Problems and the Regularization Method", *Soviet Math. Dokl.* **5** (1963) 1035/1038.

[38] V. Blobel, "An Unfolding method for high-energy physics experiments", in *Advanced statistical techniques in particle physics. Proceedings, Conference, Durham, UK, March 18-22, 2002*, pp. 258–267. 2002. arXiv:hep-ex/0208022.

[39] CMS Collaboration, "Identification of b quark jets at the CMS Experiment in the LHC Run 2", CMS Physics Analysis Summary CMS-PAS-BTV-15-001, 2016.

[40] NNPDF Collaboration, "Parton distributions for the LHC Run II", *JHEP* **04** (2015) 040, doi:10.1007/JHEP04(2015)040, arXiv:1410.8849.